厚生労働科学研究費補助金

第3次対がん総合戦略研究事業

光音響イメージングを利用した肝胆膵癌診断法の開発

平成25年度　総括研究報告書

研究代表者　　石沢 武彰

平成26（2014）年　5月

別紙１

厚生労働科学研究費補助金

第3次対がん総合戦略研究事業

光音響イメージングを利用した肝胆膵癌診断法の開発

平成25年度　総括研究報告書

研究代表者　　石沢　武彰

平成26（2014）年　5月

別紙２

目　　次

別紙３

厚生労働科学研究費補助金（第３次対がん総合戦略研究事業）
総括研究報告書

光音響イメージングを利用した肝胆膵癌診断法の開発

研究代表者　　石沢　武彰
東京大学医学部附属病院　肝胆膵・人工臓器移植外科

研究要旨：本研究では、光音響効果（感光剤を含む組織にパルスレーザーを照射すると瞬間的に熱膨張を起こし超音波を発生すること）を利用して生体構造を描出する技術（光音響イメージング）による、肝癌および膵癌の同定能を評価した。光音響イメージングによる肝癌の診断では、術前に静注された indocyanine green（ICG）を造影剤として用い、患者切除標本において肝細胞癌組織内部または腺癌組織周囲の肝実質に滞留する ICG の分布を超音波画像に重畳して３次元的に描出することが可能であった。しかし光音響シグナルの減衰のためか、組織表面から 5 mm 以深では ICG の描出が困難であり、脂肪肝発癌モデルマウスの体表から観察した光音響イメージングでも癌特異的なシグナルは検出できなかった。膵癌の光音響イメージングでは、膵癌モデルマウスの腹腔内に γ-glutamyl hydroxymethyl rhodamine green（gGlu-HMRG）を投与して撮像を試みたが、励起波長が最適化できず、またマウスでは gGlu-HMRG が膵実質に浸透し膵酵素と反応するため、癌特異的なシグナルは描出できなかった。ICG を用いた光音響イメージングは、肝癌に対する超音波検査と術中蛍光イメージングの有効性を向上させる技術として期待できるが、深部組織の描出能を改善するためには撮像技術に break through が求められる。膵癌の光音響イメージングでは新規造影剤の開発が必要である。

（研究分担者）
國土典宏　東京大学医学部附属病院
肝胆膵外科　教授
金子順一　東京大学医学部附属病院
肝胆膵外科　特任講師
清水篤志　東京大学医学部附属病院
肝胆膵外科　助教
浦野泰照　東京大学大学院医学系研究科
生体情報学講座　教授
伊地知秀明　東京大学医学部附属病院
消化器内科　助教
深山正久　東京大学大学院医学系研究科
人体病理学・病理診断学
柴原純二　東京大学大学院医学系研究科
人体病理学・病理診断学
緑川泰　日本大学医学部附属板橋病院
消化器外科　助教

A. 研究目的

近年、生体内で癌組織を蛍光標識して検査中あるいは手術中に癌組織の同定と質的診断を行うための技術が盛んに開発されている。研究代表者らは、術前に静注された indocyanine green（ICG）が肝癌組織または癌周囲の非癌部肝実質に滞留する性質を利用し、手術中に腫瘍の位置を同定する技術を開発、実臨床に応用してきた[1]。また、癌細

胞に高発現するγ-glutamyltransferaseと反応して蛍光を呈する新規プローブ（γ-glutamyl hydroxymethyl rhodamine green, gGlu-HMRG [2]）を用い、切除標本において大腸癌肝転移や胆膵癌の腺癌組織を標識できることを確認した。これらの蛍光イメージング法は高感度かつ即時反応性に優れるという長所を有す一方、組織表面の病変しか描出できないという欠点があった。

一方、この20年の間に光音響効果（金属ナノ粒子や色素を含む組織にパルスレーザーを照射すると瞬間的に熱膨張を起こし超音波を発生すること）を利用して生体構造を描出する新しいイメージング技術（光音響イメージング）が開発された[3-5]。本法は深部にある癌組織の微細な構造を描出するための技術として応用が期待されているが、これまで臨床サンプルを対象とした評価はほとんど行われていなかった。本研究の目的は、患者切除標本と発癌モデルマウスを対象とし、造影剤としてICGまたはgGlu-HMRGを用いた光音響イメージングによる肝癌・膵癌の同定能を評価することである。

B. 研究方法

1. 肝癌の光音響イメージング

i) 条件設定

・肝の構造を模した超音波検査用材料を用いてファントムを作成し、患者血清で希釈したICG溶液を封入、光音響イメージングによる信号強度を測定した。

・ヌードマウス（BALB/c）の腹部皮下にヒト高分化肝細胞癌株（HuH-7）を移植[6]。腫瘍径が5mm以上に増大した時点（移植から約10日後）でICG （5 mg/kg）を尾静脈から静注し、48時間後に蛍光イメージングと光音響イメージング（Vevo®LAZR, Visual Sonics, Toronto, ON, Canada）を行った。

ii) 患者切除標本を用いた肝癌描出能の評価

・対象は原発性肝癌または大腸癌肝転移に対し肝切除術を施行した患者9例。手術前にICG（2.5 mg/kg）を静注した[1]。肝切除後直ちに、切除標本（10結節）の蛍光イメージングと光音響イメージングを施行した。

iii) 非アルコール性脂肪性肝炎（non-alcoholic steatohepatitis, NASH）発癌モデルマウス体表撮影による肝癌同定能の評価

・NASH発癌モデルマウス（STAM™ mice, 18週齢[7]）3匹を対象とした。ICG（5mg/kg）を尾静脈から静注し、静注から48時間後に蛍光イメージングと光音響イメージングを行った。

2. 膵癌の光音響イメージング

i) 膵癌モデルマウスを用いた描出能の検討（gGlu-HMRGを使用）

・膵癌モデルマウス（膵臓上皮特異的 変異型 *Kras* 発現+*Tgfbr2* ノックアウトマウス[8]）を作成した。この膵癌モデルマウス4匹と、野生型マウス1匹、変異型 *Kras* 発現のみのPanINモデルマウス1匹に対し、gGlu-HMRG（50 μM）を腹腔内投与、イメージングを行った。

ii) 膵癌モデルマウスを用いた描出能の検討（ICGを使用）

・膵癌モデルマウス2匹に対し、ICG（5 mg/kg）を尾静脈から静注、膵組織を標的として経時的に光音響イメージングを行った。

C. 研究結果

1. 肝癌の光音響イメージング

i) 条件設定

・超音波ファントムに対する光音響イメージングでは、ICG溶液（0.001, 0.01, 0.1, 1.0 mg/mL）のうち1 mg/mLの濃度が最も信号強度が高く、濃度消光の影響を受ける蛍光イメージングの結果（0.01 mg/mLが最高値）

と乖離が見られた（図 1A)。

・ヒト肝細胞癌株皮下移植モデルマウスを用いた実験により、励起波長 800 nm, gain 54dB の条件で最もアーチファクトが抑制され、皮下腫瘤に滞留した ICG を描出できることを確認した（図 1B)。

ii) 患者切除標本を用いた肝癌描出能の評価

・肝細胞癌 5 結節、肝内胆管癌 1 結節、大腸癌肝転移 4 結節に対し、切除標本割面の蛍光イメージングを施行。肝細胞癌 4 結節で腫瘍組織に ICG の蛍光が認められた（腫瘍型)。他の 6 結節では腫瘍組織には ICG の蛍光を認めず、腫瘍周囲の非癌部肝実質がリング状の蛍光を呈した（リング型)。

・光音響イメージング（励起波長 800 nm, gain 54dB）では、蛍光イメージングで示された ICG の分布パターンが超音波画像上に 3 次元的に再現された（図 2)。しかし光音響シグナル陽性部位の信号強度は、深さ 4 mm の部位で組織表面の約 60%に減衰し、5 mm 以深では描出が困難であった。背景肝に対する腫瘍組織の信号強度の比は、腫瘍型の方がリング型よりも高かった（中央値[範囲], 1.5 [0.8-1.8] vs. 0.7 [0.5-0.8], P = 0.010 [Wilcoxon's rank-sum test])。また、背景肝に対する癌周囲の非癌部肝実質の信号強度の比は、腫瘍型よりもリング型の方が高かった（0.8 [0.7-1.0] vs. 1.3 [1.1-1.5], P = 0.010)。

iii) NASH 発癌モデルマウス体表撮影による肝癌同定能の評価

・ICG を静注した NASH 発癌モデルマウス体表から上記の条件で光音響イメージングを行ったが、超音波画像で同定される肝腫瘍内に癌特異的な光音響シグナルは描出されなかった（図 3A)。

・肝摘出後に肝表面および肝割面を観察すると、計 10 結節の癌組織が同定された。蛍光イメージングでは 10 結節中 4 結節に ICG の蛍光が確認された（図 3B)。

2. 膵癌の光音響イメージング

i) 膵癌モデルマウスを用いた描出能の検討（gGlu-HMRG を使用）

・先の超音波ファントムに HMRG を封入し光音響イメージングで撮像したが、設定可能域下限の励起波長（680 nm）でプローブ特異的な信号が検出されなかった。

・gGlu-HMRG を腹腔内投与した膵癌モデルマウスおよび野生型マウス体表から行った光音響イメージングでは、いずれの個体においても膵内に光音響シグナルを検出できなかった。

・開腹後に行った腹腔内の蛍光イメージングでは、野生型および PanIN モデルマウスでは非癌部の膵実質が強い蛍光を呈したのに対し、膵癌モデルマウスでは膵組織に蛍光シグナルが観察されなかった（図 4)。

ii) 膵癌モデルマウスを用いた描出能の検討（ICG を使用）

・Magnetic resonance imaging で癌化が確認された膵体尾部領域に関心領域を設定し、ICG 静注後 15 分まで光音響イメージングで観察したが、腫瘍特異的な信号強度の上昇は検出されなかった。

D. 考察

本研究では、すでに実臨床に導入されている ICG 蛍光イメージングの理論を応用し、先端光学技術である光音響イメージングを臨床サンプル（患者切除標本）の評価に適用して癌組織を描出できることが示された。腫瘍の組織像と光音響イメージとの関連では、肝細胞癌 4 結節で腫瘍組織に滞留する ICG が描出され、腺癌組織 5 結節を含む残りの 6 結節では腫瘍周囲の非癌部肝実質に ICG のシグナルがリング状に同定された。これらの光音響シグナルは、肝癌の割面における蛍光

イメージングの結果[9]と一致した。光音響イメージングは、超音波画像上にICGなどの造影剤の分布をリアルタイムに表示できるという利点を持つ。超音波検査は肝腫瘍のスクリーニングおよび術中診断に不可欠な画像検査法として広く普及しており、光音響イメージングは超音波画像に胆汁排泄などに関する機能的な情報を付加する技術として臨床応用される可能性がある。

光音響イメージングは、理論的には組織表面から7 cm程度までシグナルの検出が可能であるとされている[10]。しかし本研究で用いた撮像装置と撮像条件の下では、組織深部に滞留したICGから発せられる光音響シグナルの描出が不十分であった。組織内、特に皮膚を透過する際のシグナルの減衰が主な原因であると考えられるが、組織中のICGの濃度が蛍光イメージングには最適であるものの光音響イメージングには不十分であった可能性もある。今後、光音響イメージングによる肝腫瘍の検出限界を改善すべく、励起レーザー光の出力と信号検出の感度向上、およびICG投与法の最適化を図る必要がある。

本研究では、ヒト腺癌組織に高発現するγ-glutamyltransferaseと反応して蛍光を呈するgGlu-HMRGを腹腔内投与し、蛍光イメージングと同時に光音響イメージングで膵癌組織を描出することを試みたが、今回使用した光音響イメージング装置のレーザー波長（最短 680 nm）では、HMRG（蛍光イメージングにおける励起波長 490 nm）の光音響シグナルは検出できなかった。またマウスではgGlu-HMRGが非癌部の膵実質に浸透し膵酵素と反応するためか、gGlu-HMRGに対する蛍光イメージングでも膵癌組織はむしろ陰性像として描出された。さらにICG静注による光音響イメージングでも、膵癌組織および非癌部膵実質における血流分布の相違を描出することはできなかった。光音響イメージングを膵癌の診断に応用するためには、膵癌組織に特異的に分布し、かつ十分な光音響シグナルを発する新規造影剤の開発が必要である。

E. 結論

ICGを用いた光音響イメージングは、肝癌に対する超音波検査と術中蛍光イメージングの有効性を向上させる技術として期待できるが、深部に位置する腫瘍の描出能を改善するためにはICG投与法の最適化と撮像技術の進歩が求められる。膵癌組織に特異的に分布し、かつ十分な光音響シグナルを発するプローブが開発されれば、光音響イメージングは膵癌のスクリーニングにも応用できる可能性がある。

F. 健康危険情報

該当なし

G. 研究発表

1. 論文発表

・Ishizawa T, Masuda K, Urano Y, Kawaguchi Y, Satou S, Kaneko J, Hasegawa K, Shibahara J, Fukayama M, Tsuji S, Midorikawa Y, Aburatani H, Kokudo N. Mechanistic background and clinical applications of indocyanine green fluorescence imaging of hepatocellular carcinoma. Annals of Surgical Oncology 2014;21:440-8.

・Ishizawa T, Kokudo N. The beginning of a new era of digestive surgery guided by fluorescence imaging. Liver Cancer 2014;3:6-8.

・Kudo H, Ishizawa T, Tani K, Harada N, Ichida A, Shimizu A, Kaneko J, Aoki T,

Sakamoto Y, Sugawara Y, Hasegawa K, Kokudo N. Visualization of subcapsular hepatic malignancy by indocyanine-green fluorescence imaging during laparoscopic hepatectomy. Surgical Endoscopy (in press)

2. 学会発表

・Real-time visualization of pancreatic leak using a chymotrypsin-activated fluorescent probe during pancreatic surgery. SPIE BiOS, San Francisco, California, US, 2014

・Rapid and Sensitive Imaging of Cancer Cells in Resected Human Live Tissues by Novel Fluorescence Probes for γ-glutamyltranspeptidase. The 13th Annual Surgery of the Foregut Symposium, Florida, US, 2014

H. 知的財産権の出願・登録情報

1. 特許取得: なし
2. 実用新案登録: なし
3. その他: なし

（参考文献）

1. Ishizawa T, Fukushima N, Shibahara J, et al.: Real-time identification of liver cancers by using indocyanine green fluorescent imaging. Cancer 2009;115:2491-504.
2. Urano Y, Sakabe M, Kosaka N, et al. Rapid cancer detection by topically spraying a γ-glutamyltranspeptidase -activated fluorescent probe. Sci Transl Med 2011; 3: 110-19.
3. Kruger RA. Photoacoustic ultrasound. Med Phys 1994;21:127-31.
4. Oraevsky AA, Jacques SL, Tittel FK. Measurement of tissue optical properties by time-resolved detection of laser-induced transient stress. Appl Opt 1997;36:402-15.
5. Wang LV. Multiscale photoacoustic microscopy and computed tomography. Nat Photonics 2009;3:503-9.
6. Kaneko J, Inagaki Y, Ishizawa T, et al. Photodynamic therapy for human hepatoma-cell-line tumors utilizing biliary excretion properties of indocyanine green. J Gastroenterol 2014;49:110-6.
7. Fujii M, Shibazaki Y, Wakamatsu K, et al. A murine model for non-alcoholic steatohepatitis showing evidence of association between diabetes and hepatocellular carcinoma. Med Mol Morphol 2013;46:141-52.
8. Ijichi H1, Chytil A, Gorska AE, et al. Aggressive pancreatic ductal adenocarcinoma in mice caused by pancreas-specific blockade of transforming growth factor-beta signaling in cooperation with active Kras expression. Genes Dev 2006;20:3147-60.
9 Ishizawa T, Masuda K, Urano Y, et al. Mechanistic background and clinical applications of indocyanine green fluorescence imaging of hepatocellular carcinoma. Ann Surg Oncol 2014;21:440-8.
10. Wang LV, Hu S. Photoacoustic tomography: in vivo imaging from organelles to organs. Science 2012; 23;335:1458-62.

図1 ICGを用いた光音響イメージングの基礎的検討

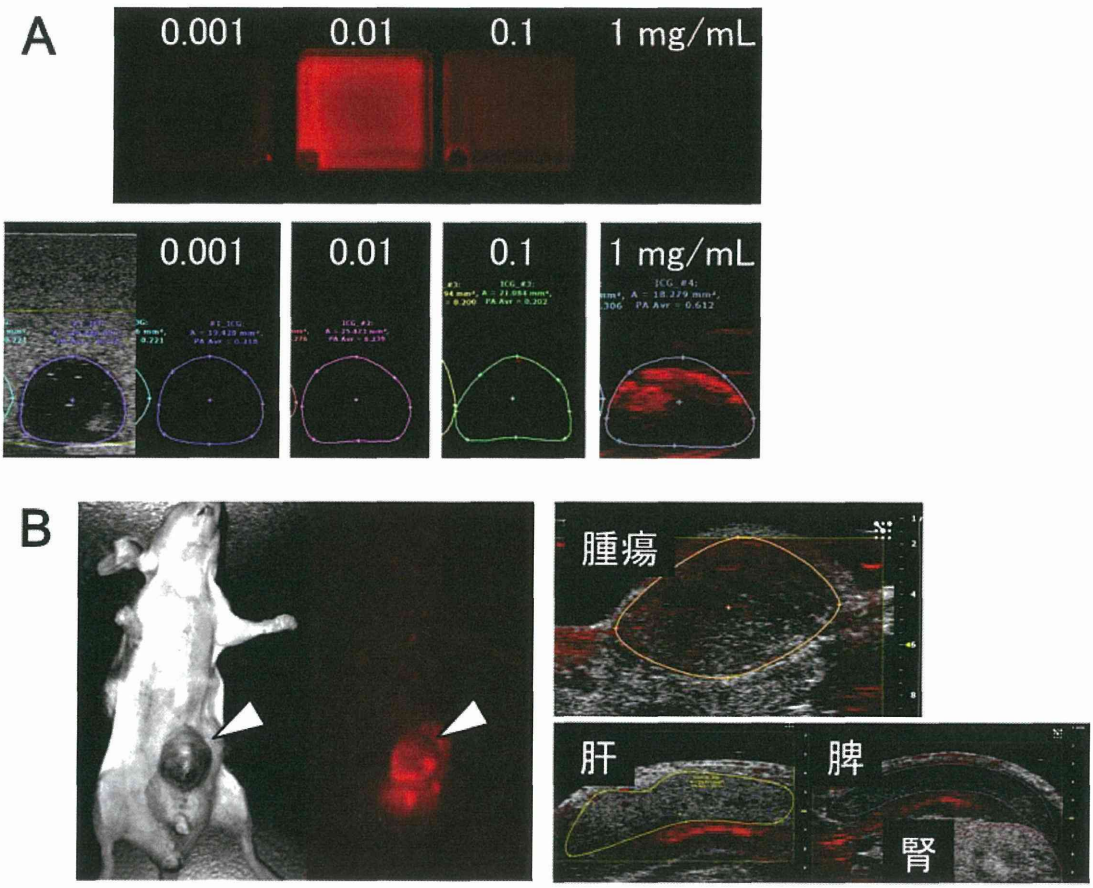

(A) 蛍光観察では0.01 mg/mLのICG溶液が最も強い蛍光を呈したが（上段)、光音響イメージングでは1 mg/mLのICG溶液で信号強度が最大となった。
(B) ヒト高分化肝細胞癌株皮下移植モデルの蛍光像（左，矢頭は腫瘍）と光音響イメージング（右)。平均信号強度は腫瘍 0.34，肝 0.23，脾 0.26，腎 0.19 (a.u.)。

図２　肝切除標本における腫瘍と背景肝の光音響イメージング

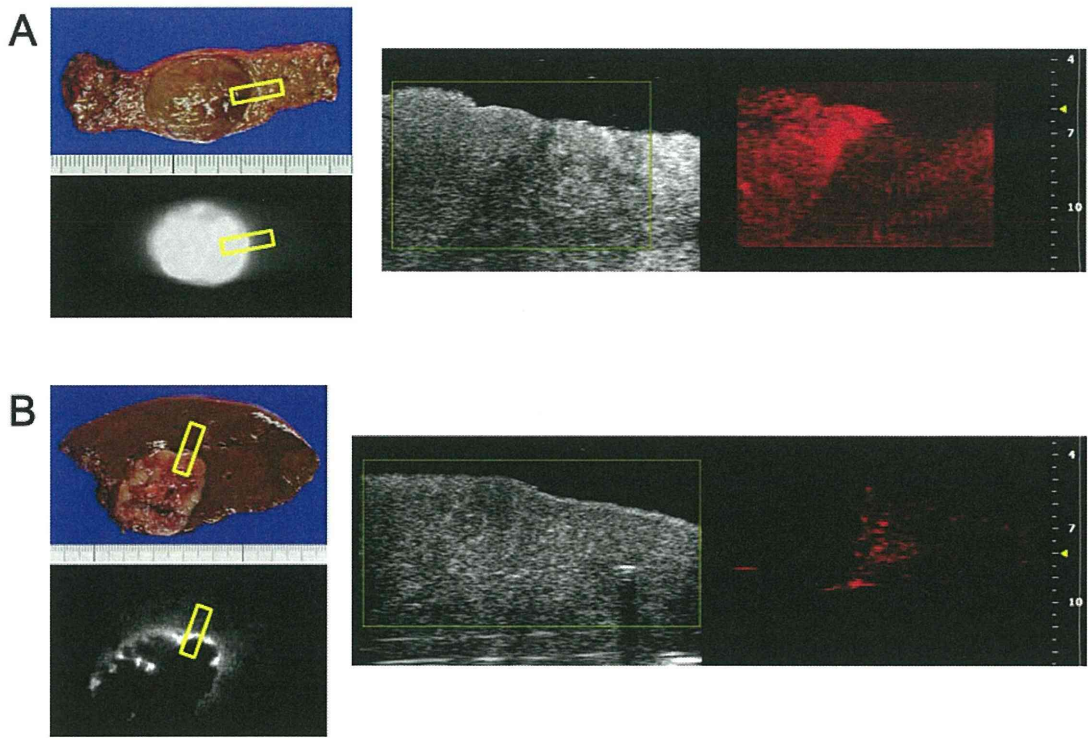

(A) 肝細胞癌の肉眼像（左上)、ICG 蛍光像（左下)、黄色枠部分で撮影した光音響イメージング（右，腫瘍に滞留した ICG が高信号を呈している)。(B) 大腸癌肝転移の肉眼像、ICG 蛍光像、および光音響イメージング（腫瘍周囲に滞留した ICG が高信号を呈している)。

図３　NASH 発癌モデルの光音響イメージング

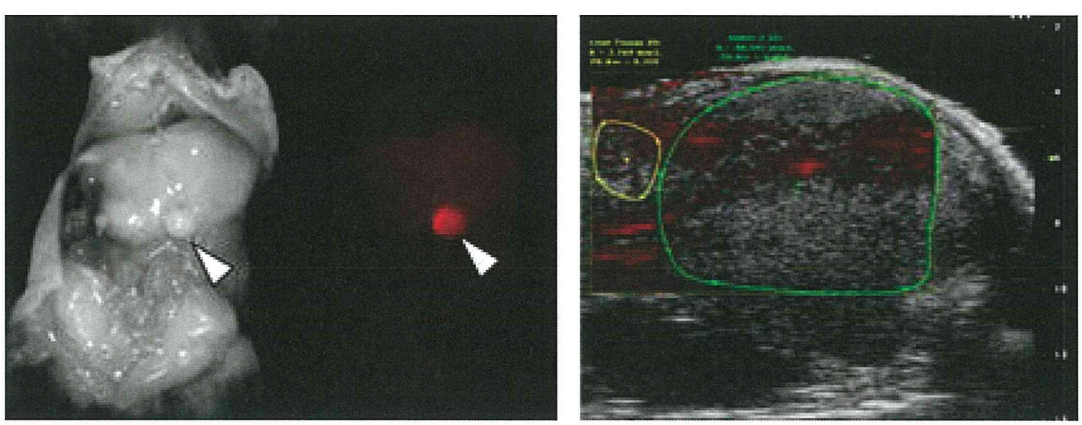

開腹後の蛍光イメージング（左）では腫瘍に集積した ICG が描出されるが（矢頭)、
体表からの光音響イメージング（右）では腫瘍特異的な ICG の信号は検出されなかった。

図４　gGlu-HMRG を用いた膵癌モデルマウスの蛍光イメージング

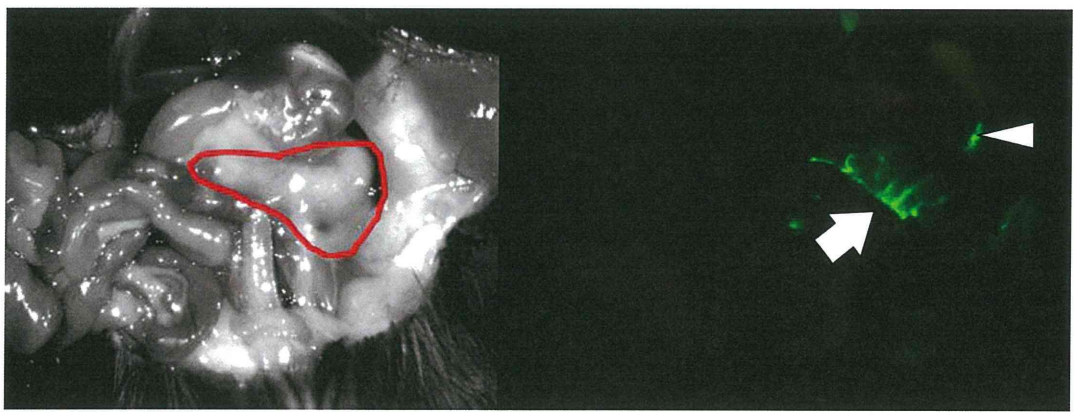

膵癌モデルマウスに gGlu-HMRG を腹腔内投与し 10 分後に開腹、励起波長 600 nm で撮影した白色光画像（左、膵を赤枠で示す）と蛍光像（右）。蛍光像では非癌部と思われる膵組織が gGlu-HMRG と反応し蛍光を呈している（矢印）。胆汁と反応するためか胆嚢も蛍光を呈している（矢頭）。

別紙４

研究成果の刊行に関する一覧表

書籍

著者氏名	論文タイトル名	書籍全体の編集者名	書　籍　名	出版社名	出版地	出版年	ページ
なし							

雑誌

発表者氏名	論文タイトル名	発表誌名	巻号	ページ	出版年
Ishizawa T,Urano Y, Shibahara J, Fukayama M, Midorikawa Y, Kokudo N, et al.	Mechanistic background and clinical applications of indocyanine green fluorescence imaging of hepatocellular carcinoma.	Annals of Surgical Oncology	21	440-448	2014
Ishizawa T, Kokudo N.	The beginning of a new era of digestive surgery guided by fluorescence imaging.	Liver Cancer	3	6-8	2014
Kudo H, Ishizawa T, Shimizu A, Kokudo N, et al.	Visualization of subcapsular hepatic malignancy by indocyanine-green fluorescence imaging during laparoscopic hepatectomy.	Surgial Endoscopy			(in press)

Ann Surg Oncol
DOI 10.1245/s10434-013-3360-4

Annals of
SURGICAL ONCOLOGY
OFFICIAL JOURNAL OF THE SOCIETY OF SURGICAL ONCOLOGY

ORIGINAL ARTICLE – HEPATOBILIARY TUMORS

Mechanistic Background and Clinical Applications of Indocyanine Green Fluorescence Imaging of Hepatocellular Carcinoma

Takeaki Ishizawa, MD,PhD[1], Koichi Masuda, MD[1], Yasuteru Urano, PhD[2], Yoshikuni Kawaguchi, MD[1], Shouichi Satou, MD,PhD[1], Junichi Kaneko, MD,PhD[1], Kiyoshi Hasegawa, MD,PhD[1], Junji Shibahara, MD,PhD[3], Masashi Fukayama, MD,PhD[3], Shingo Tsuji, PhD[4], Yutaka Midorikawa, MD,PhD[4], Hiroyuki Aburatani, MD,PhD[4], and Norihiro Kokudo, MD,PhD[1]

[1]Hepato-Biliary-Pancreatic Surgery Division, Department of Surgery, University of Tokyo, Tokyo, Japan; [2]Laboratory of Chemical Biology and Molecular Imaging, University of Tokyo, Tokyo, Japan; [3]Department of Pathology, Graduate School of Medicine, The University of Tokyo, Tokyo, Japan; [4]Genome Science Division, Research Center for Advanced Science & Technology, The University of Tokyo, Tokyo, Japan

ABSTRACT

Background. Although clinical applications of intraoperative fluorescence imaging of liver cancer using indocyanine green (ICG) have begun, the mechanistic background of ICG accumulation in the cancerous tissues remains unclear.

Methods. In 170 patients with hepatocellular carcinoma cells (HCC), the liver surfaces and resected specimens were intraoperatively examined by using a near-infrared fluorescence imaging system after preoperative administration of ICG (0.5 mg/kg i.v.). Microscopic examinations, gene expression profile analysis, and immunohistochemical staining were performed for HCCs, which showed ICG fluorescence in the cancerous tissues (cancerous-type fluorescence), and HCCs showed fluorescence only in the surrounding non-cancerous liver parenchyma (rim-type fluorescence).

Results. ICG fluorescence imaging enabled identification of 273 of 276 (99 %) HCCs in the resected specimens. HCCs showed that cancerous-type fluorescence was associated with higher cancer cell differentiation as compared with rim-type HCCs ($P < 0.001$). Fluorescence microscopy identified the presence of ICG in the canalicular side of the cancer cell cytoplasm, and pseudoglands of the HCCs showed a cancerous-type fluorescence pattern. The ratio of the gene and protein expression levels in the cancerous to non-cancerous tissues for Na^+/taurocholate cotransporting polypeptide (NTCP) and organic anion-transporting polypeptide 8 (OATP8), which are associated with portal uptake of ICG by hepatocytes that tended to be higher in the HCCs that showed cancerous-type fluorescence than in those that showed rim-type fluorescence.

Conclusions. Preserved portal uptake of ICG in differentiated HCC cells by NTCP and OATP8 with concomitant biliary excretion disorders causes accumulation of ICG in the cancerous tissues after preoperative intravenous administration. This enables highly sensitive identification of HCC by intraoperative ICG fluorescence imaging.

Real-time cancer identification using fluorescence probes currently represents one of the most active research fields. In comparison with the enormous amount of basic research, however, there are very few techniques that are applicable in clinical settings. The application of fluorescence imaging is still being limited to the identification of glioblastoma,[1] bladder cancer,[2] and skin tumors,[3] using the porphyrin precursor 5-aminolevulinic acid. Fluorescence imaging is also limited in identifying the present subject of the intraoperative delineation of liver cancer using indocyanine green (ICG).[4,5]

Protein-bound ICG emits light that peaks at approximately 840 nm when illuminated with near-infrared light (750–810 nm).[6] This fluorescence property of ICG was

Takeaki Ishizawa and Koichi Masuda equally contributed as first authors.

Electronic supplementary material The online version of this article (doi:10.1245/s10434-013-3360-4) contains supplementary material, which is available to authorized users.

First Received: 10 July 2013

N. Kokudo, MD,PhD
e-mail: kokudo-2su@h.u-tokyo.ac.jp

Published online: 20 November 2013

already revealed in detail in the 1970s, and real-time fluorescence imaging using ICG began clinical application in the early 1990s to fundus angiography in the field of ophthalmology.[7] In the twenty-first century, the application of ICG fluorescence imaging was extended to surgery as an intraoperative navigation tool of lymphatic flow,[8] sentinel lymph nodes,[9] and blood flow during coronary artery bypass grafting [10] and clipping of cerebral aneurysm.[11] However, probably because ICG has been widely adopted as a reagent for measuring liver function instead, little attention has been paid to the fluorescence property of ICG in the fields of digestive surgery until Japanese groups developed intraoperative fluorescence cholangiography[12,13] focusing on another property of ICG (i.e., biliary excretion).

Originally, Ishizawa et al. developed fluorescence cholangiography using ICG during open surgery,[12] and then during laparoscopic surgery.[13] In this process, we noticed that the tumors on the liver surface emitted their own fluorescence, even before ICG was injected into the bile duct for cholangiography. Actually, with all of the patients in our department, ICG is intravenously administered prior to surgery to measure the ICG retention rate at 15 min (ICGR15) for estimating the maximum limit of the hepatic volume to be resected safely.[14,15] Thus, we hypothesized that liver cancer could be identified by fluorescence imaging through visualization of the ICG that remained in the cancerous tissues and/or surrounding liver tissues after preoperative intravenous injection.[4] The ICG fluorescence imaging of liver cancer has been recently applied as an intraoperative navigation.[16] However, the mechanism of ICG accumulation in liver cancer tissues remains unclear. Here, we reveal the pharmacokinetics of ICG in HCC tissues, which can explain the differences in the fluorescence patterns by the results of microscopic examinations and gene expression profiling, and discuss the expected role of fluorescence imaging as an intraoperative cancer navigation tool in the clinical setting.

METHODS

Patients

This study was conducted with the approval of the institutional ethics review board. There were 170 patients who had undergone liver resection for HCC at the University of Tokyo Hospital between July 2007 and July 2011. Preoperative diagnosis of HCC was made according to the following procedures: all patients underwent abdominal ultrasonography, contrast-enhanced helical computed tomography (CT), and magnetic resonance imaging (MRI) using gadolinium ethoxybenzyl diethylenetriamine pentaacetic acid. Resection was indicated for tumors in which CT and/or MRI examination revealed both early hyper-enhancement and delayed hypo-enhancement. Surgical procedures were determined according to a decision tree indicating the acceptable limit of the resected liver volume, based on the preoperative ICG retention rate at 15 min (ICGR15).[14]

ICG Fluorescence Imaging of the Liver Surface and Resected Specimens

The technical details of ICG fluorescence imaging have been previously described.[4] Briefly, ICG (Diagnogreen, Daiichi Sankyo, Tokyo, Japan), which had been injected at a dose of 0.5 mg/kg i.v. within 2 weeks, in principle, prior to surgery, was used as the fluorescent source. Intraoperatively, fluorescence images of the liver surface were obtained by a commercially available fluorescence imaging system (PDE, Hamamatsu Photonics, Hamamatsu, Japan) before resection, but after visual inspection, manual palpation, and contrast-enhanced intraoperative ultrasonography (IOUS) using perfluorobutane microbubbles (Sonazoid, GE Healthcare, Oslo, Norway).[17] New lesions identified by ICG fluorescence imaging were resected if they were also detected by subsequent IOUS and the additional resection was technically feasible. After the resection, the surgical specimens were sliced into approximately 10-mm sections in the operating room. All of the cut surfaces were investigated using the fluorescence imaging system. Any fluorescing lesions larger than 5 mm in diameter were marked with needles and were examined by experienced pathologists (J.S. and M.F.) according to the Japanese classification system [18] and the criteria proposed by the International Working Party.[19]

Fluorescence Microscopy, Bioinformatics Analysis, and Immunohistochemical Staining

The fluorescent intensity (FI) of the lesions and noncancerous liver tissues was evaluated with specific software (U11437, Hamamatsu Photonics) and the lesion-to-liver contrast was calculated by subtracting the FI of the noncancerous liver parenchyma from that of the lesion. Fluorescence microscopic examinations were also performed using the Nuance multispectral imaging system (CRi, Woburn, MA). Bioinformatics analysis and immunohistochemical staining were added on to the resected specimens in the consecutive 32 patients examined during the latter period of the study (see details in the Supplementary Methods).

Statistical Analysis

Continuous data were expressed as median (range). Quantitative and categorized variables were compared using the Wilcoxon's rank-sum test and the Fisher's exact test, respectively. The survival curves were estimated using

TABLE 1 Background characteristics of patients with HCCs

	HCCs showing cancerous-type fluorescence of ICG ($n = 240$)	HCCs showing rim-type fluorescence of ICG ($n = 33$)	P
Hepatitis B surface antigen, positive	62 (26 %)	16 (48 %)	0.012
Hepatitis C virus antibody, positive	109 (45 %)	11 (33 %)	0.262
Child-Pugh class, B or C	11 (5 %)	0 (0 %)	0.370
Background liver, cirrhosis	101 (42 %)	8 (24 %)	0.058
Preoperative ICGR15 (%)[a]	13.0 (3.3–46.5)	10.4 (3.3–29.6)	0.131
Interval between ICG injection and surgery (days)[a]	4 (1–25)	4 (1–21)	0.070
Cancer cell differentiation			
Well	67 (28 %)	1 (3 %)	<0.001[b]
Moderate	168 (70 %)	14 (42 %)	
Poor	5 (2 %)	18 (55 %)	
Microscopic vascular invasion, present	78 (33 %)	18 (55 %)	0.019
Tumor size (mm)[a]	16 (2–210)	23 (6–90)	0.030
α-Fetoprotein level (ng/mL)[a]	11 (0.8–139,921)	17 (0.8–17,530)	0.332
Des-γ-carboxy prothrombin (mAu/mL)[a]	64 (4.5–61,435)	62 (15–27,193)	0.375

HCCs showing the cancerous-type fluorescence pattern of ICG includes the total and partial types of fluorescence

HCCs hepatocellular carcinoma cells, *ICG* indocyanine green, *ICGR15*, indocyanine green retention rate at 15 min

[a] Median (range)

[b] Pearson's Chi square test

the Kaplan–Meier method and compared using the log-rank test. P values <0.05 were considered to show statistical significance. Statistical analysis was performed using the JMP software (version 9.0.0; SAS Institute Inc., Cary, NC).

RESULTS

Cancer Detectability by ICG Fluorescence Imaging of the Resected Specimens

ICG fluorescence imaging identified 273 of 276 HCCs (sensitivity, 99 %). The fluorescence patterns were classified into cancerous-type fluorescence [cancer tissues showing uniform ($n = 130$) or partial ($n = 110$) fluorescence] and rim-type fluorescence (only the surrounding liver parenchyma showing fluorescence, $n = 33$) (Supplementary Fig. 1).[4] In the three patients with these false-negative results of ICG fluorescence imaging, the intervals between the intravenous injection of ICG and surgery were 24, 50, and 52 days, which were exceptionally long when compared with those in the remaining 167 patients (median, 3 days; range, 1–25 days). HCCs that showed cancerous-type fluorescence were associated with higher cancer cell differentiation, as well as those with lower incidence of hepatitis B virus infection, smaller tumor diameter, and lower incidence of microscopic vascular invasion, as compared with rim-type HCCs (Table 1).

Among the 273 HCCs that were detected by ICG fluorescence imaging, 21 tumors (13 well-differentiated and 8 moderately differentiated HCCs) were not identifiable by gross examination (Fig. 1a, b). ICG fluorescence imaging also revealed positive fluorescence in 16 non-cancerous (false-positive) lesions (large regenerative nodule, $n = 7$; dysplastic nodule, $n = 3$; bile duct proliferation, $n = 3$; necrosis, $n = 1$; no lesion, $n = 2$). The positive predictive value of ICG fluorescence imaging was 94 % (Fig. 1c). The 21 HCCs that were unidentifiable by gross inspection showed a larger tumor diameter and higher FI than the 16 non-cancerous lesions [7 (5–12) vs. 5 (5–7) mm ($P = 0.001$); 194 (135–255) arbitrary unit (au) vs. 112 (30–193) au ($P < 0.001$), respectively] (Fig. 1d).

Identification of Gene Sets Associated with the ICG Fluorescence Pattern

We applied gene set enrichment analysis (GSEA)[20] to 26 HCC samples (excluding 6 inadequate samples for RNA extraction) for the identification of gene sets associated with the ICG fluorescence pattern. First, the expression data from 20 lesions showing cancerous-type fluorescence and 6 lesions showing rim-type fluorescence patterns were extracted, and GSEA identified 95 gene sets that were significantly associated with the fluorescence patterns (Supplementary Fig. 2). Among these gene sets, a GSEA set, which was originally selected as deregulated in hepatoblastoma and liver cancer development, exhibited the most significant enrichment of all

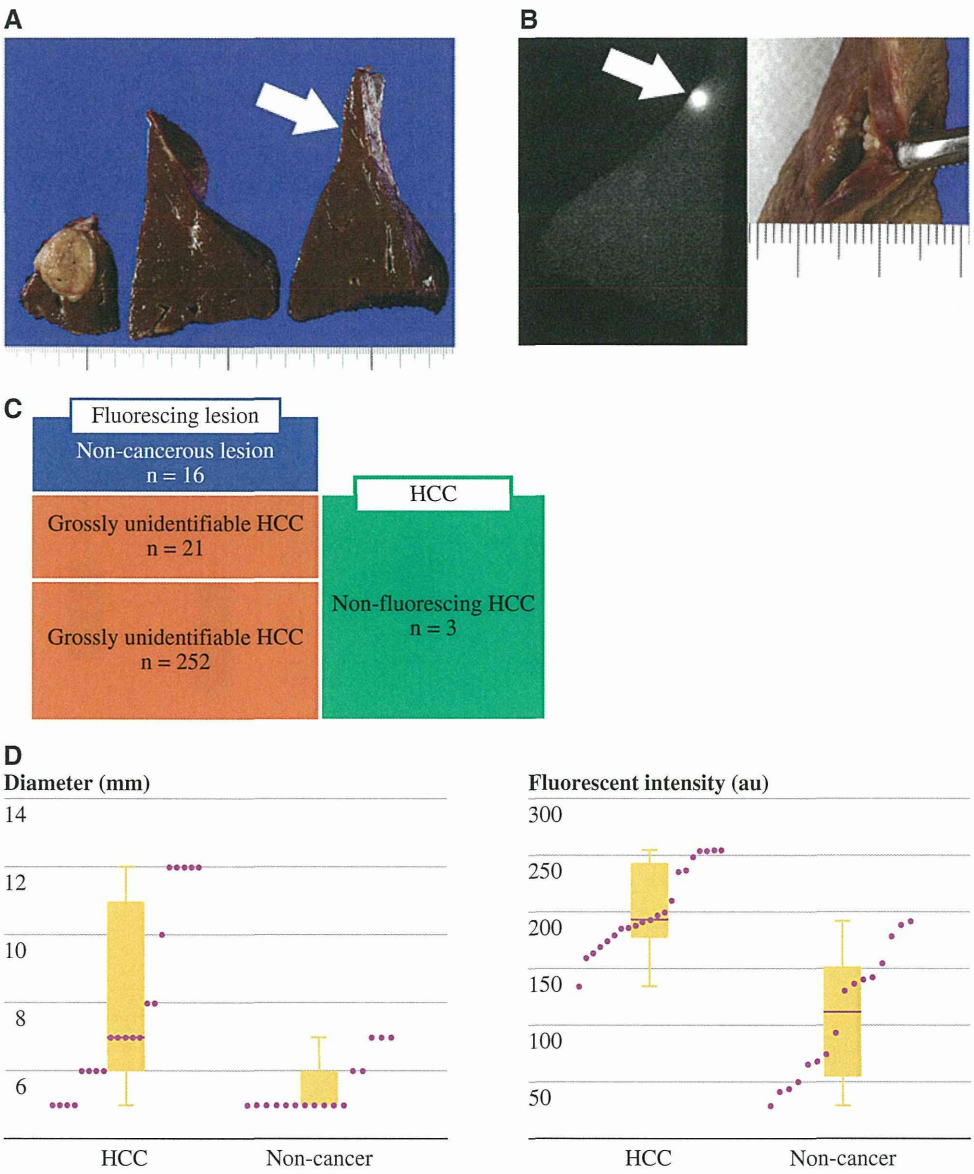

FIG. 1 Identification of new lesions in the resected specimens by ICG fluorescence imaging. Fluorescence imaging on the cut surfaces of the surgical specimens after hepatic segmentectomy (**a**) delineated a fluorescing lesion apart from the main tumor that had not been preoperatively diagnosed (see *arrows* in **a**, **b**). Additional incision of the fluorescing lesion revealed an intrahepatic metastasis of the hepatocellular carcinoma cell (HCC) (**b**, *right*). **c** Indocyanine green (ICG) fluorescence imaging identified 273 of 276 HCCs (sensitivity, 99 %). Among them, 21 could only be detected by fluorescence imaging and not by gross visual inspection. ICG fluorescence imaging also revealed fluorescence from 16 non-cancerous lesions (positive predictive value, 94 %). **d** Among the 37 lesions, in total, that could not be identified by gross inspection, the tumor diameter was larger (*left*) and the FI were higher (*right*) in the 21 HCCs than in the 16 non-cancerous lesions [7 (5–12) vs. 5 (5–7) mm, $P = 0.001$; and 194 (135–255) au vs. 112 (30–193) au, $P < 0.001$, respectively]

queried genes.[21] Then, we focused on the gene sets identified by Cairo et al.,[21] which included genes encoding organic anion-transporting polypeptides (*OATP8* [also known as *SLCO1B3*], *OATP-B* [*SLCO2B1*], *OATP-C* [*SLCO1B1*]), *NTCP* [*SLC10A 1*]), intracellular transporters (*GSTT1*, *GSTT2*, *GSTM1*, *GSTP1*), and export transporters expressed on the sinusoidal side (*MRP1* [*ABCC1*], *MRP3* [*ABCC3*]) or the canalicular side (*MRP2* [*ABCC2*]) of hepatocytes.

Expression data indicated that the ratio of the gene expressions in the cancerous tissues to non-cancerous liver tissues (C/N ratio) tended to be higher in HCCs showing the cancerous-type fluorescence pattern of ICG ($n = 13$) than in those showing the rim-type fluorescence ($n = 6$) for *NTCP* and *OATP8*, which are associated with the portal uptake of ICG by the hepatocytes,[22] as well as for *OATP-C*, *MRP2*, and *GSTT1* (Fig. 2). The C/N ratios of the other genes associated with intracellular transport (*GSTT2*, *GSTM1*, *GSTP1*) or excretion (*MRP1*, *MRP3*) of organic anions did not differ according to the presence/absence/type of ICG fluorescence in the HCCs.

Immunohistochemical Staining

Fluorescence microscopy demonstrated the fluorescence of ICG retained in the cytoplasm and pseudoglands in the cancerous tissues of both HCCs showing the total- and partial-type fluorescence and in the non-cancerous liver parenchyma surrounding the HCCs showing rim-type fluorescence (Fig. 3a).

Immunostaining for NTCP and OATP8 was performed in 32 of 276 HCCs. In the non-cancerous liver parenchyma, NTCP and OATP8 were expressed on the cellular membrane

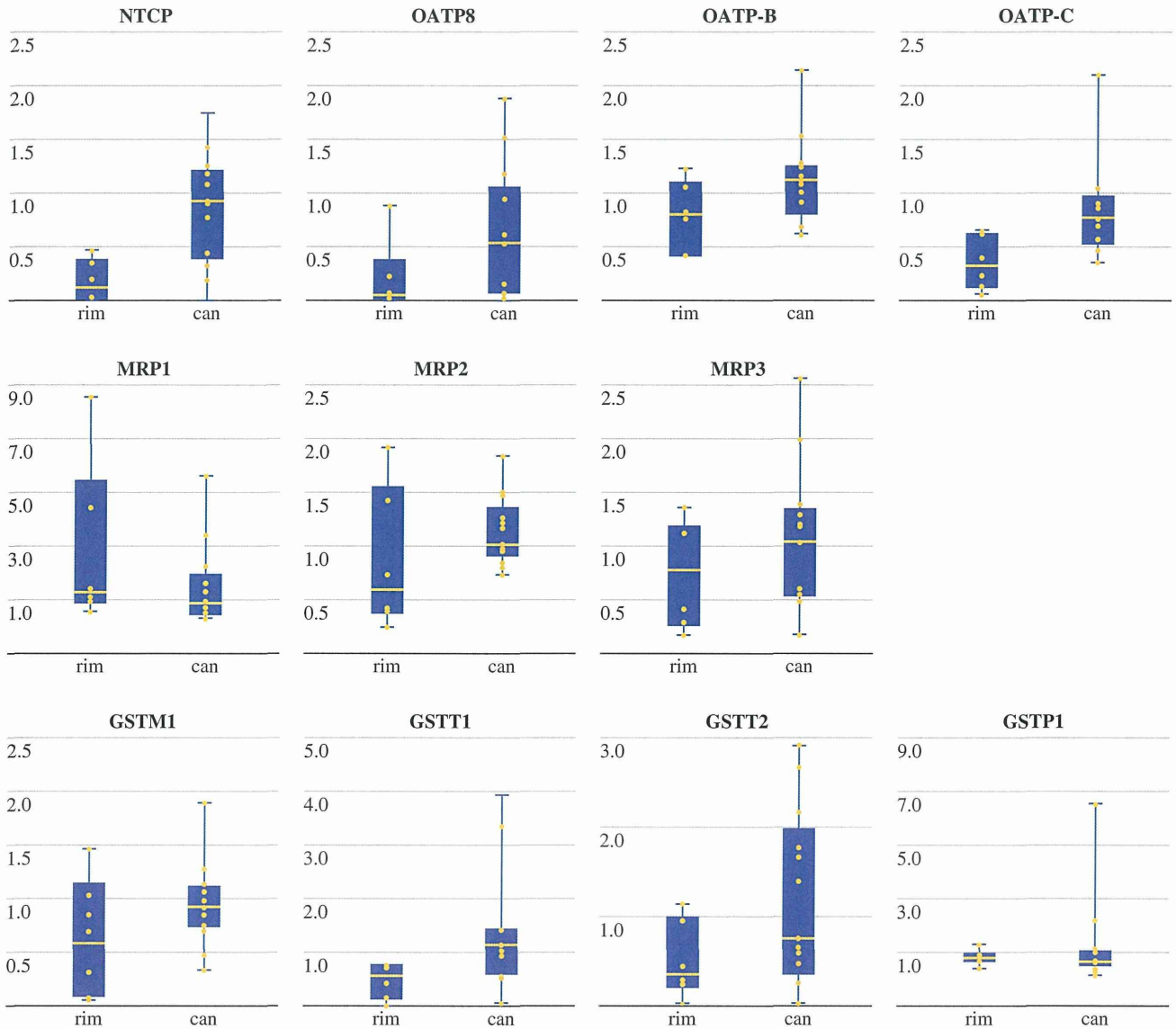

FIG. 2 The cancerous tissues to non-cancerous liver tissues (C/N) ratios of the hepatic transporters between HCCs showing cancerous-type fluorescence of indocyanine green (ICG) (can) and HCCs showing rim-type fluorescence (rim). The C/N ratio tended to be higher in the 13 HCCs showing cancerous-type fluorescence of ICG than in the 6 showing rim-type fluorescence ($n = 6$) for Na^+/taurocholate cotransporting polypeptide (*NTCP*) [0.93 (<0.01–1.75) vs. 0.12 (0.01–0.47)], *OATP8* [0.54 (<0.01–1.89) vs. 0.06 (<0.01–0.89)], *OATP-C* [0.78 (0.36–2.10) vs. 0.33 (0.07–0.66)], *MRP2* [1.02 (0.74–1.83) vs. 0.59 (0.25–1.92)], and *GSTT1* [1.13 (0.05–3.36) vs. 0.56 (< 0.01–0.78)]. Whiskers indicate the median (25th to 75th percentile) with range

of the hepatocytes, at the sinusoidal side. The NTCP and OATP8 expression levels in the cancerous tissues were higher in the 23 HCCs showing cancerous-type fluorescence of ICG than in the 9 that showed rim-type fluorescence ($P = 0.010$ and $P = 0.044$, respectively). However, the intensity of OATP8 staining was weaker than that of NTCP (Fig. 3b–d).

Applications of ICG Fluorescence Imaging to Liver Resection

Based on ICG fluorescence imaging of the liver surface before resection, 21 fluorescing lesions (19 patients) that were not detected by preoperative imaging were additionally resected. Among these, 14 lesions were pathologically confirmed to be HCC (Fig. 4a) and the remaining 7 lesions were false-positives (large regenerative nodules, $n = 4$; and no lesions, $n = 3$).

Intraoperative ICG fluorescence imaging before resection also enabled identification of 3 HCCs, which had been diagnosed by preoperative contrast-enhanced CT, but was not identifiable during surgery by visual inspection, manual palpation, fundamental IOUS, or contrast-enhanced IOUS (Fig. 4b). After liver resection, fluorescence imaging identified residual fluorescing lesions on the raw surface of the

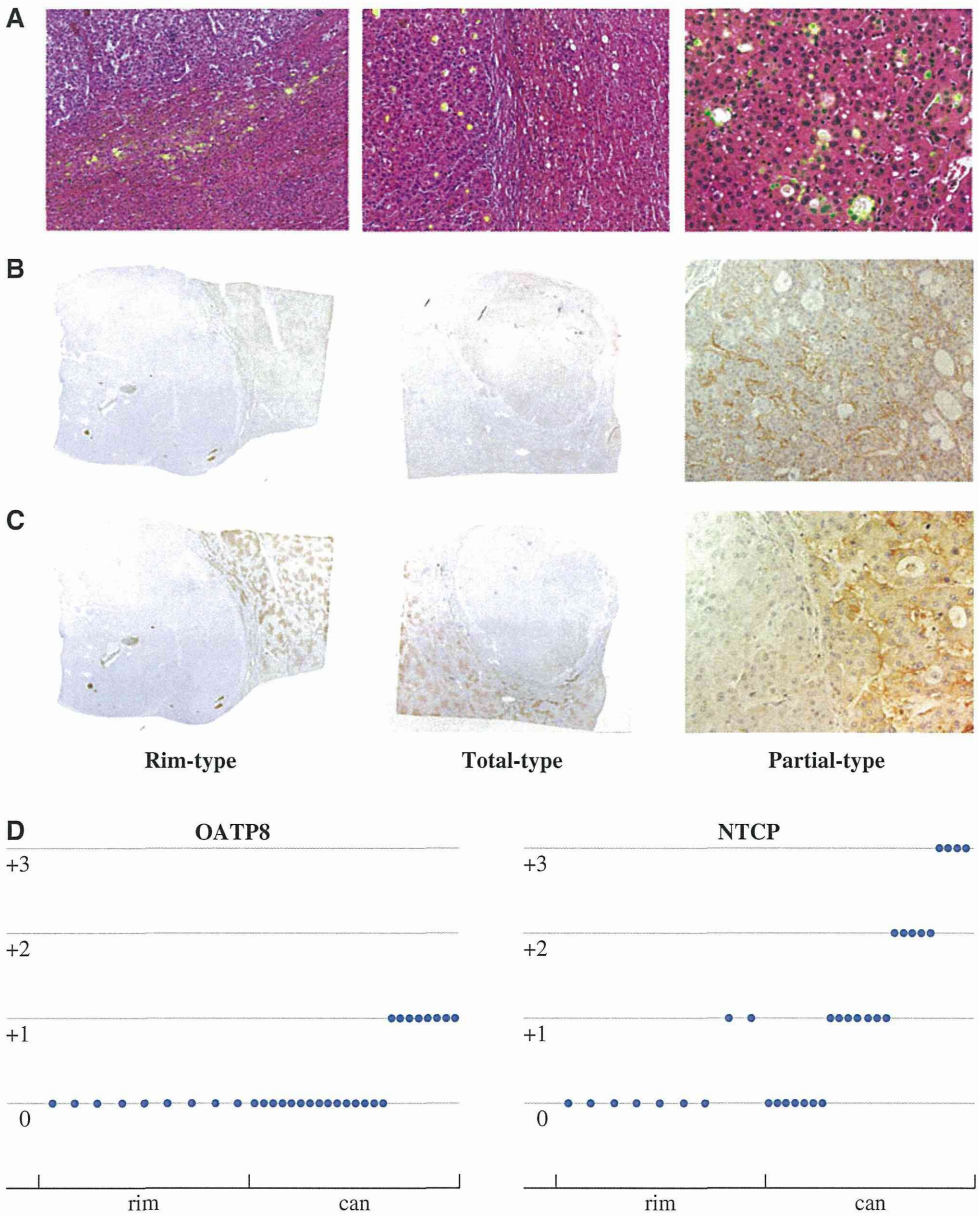

FIG. 3 Microscopic examinations. **a** Fluorescence microscopy. Fluorescence of indocyanine green (ICG) (*green*) is detected in the non-cancerous liver parenchyma around the tumor in the HCCs showing rim-type fluorescence (*left*) and in the pseudoglands and canalicular side of the cellular cytoplasm of the cancerous tissues in the HCCs showing total-type (*middle*) or partial-type fluorescence (*right*). **b** Immunohistochemical staining of Na^+/taurocholate cotransporting polypeptide (NTCP). Cancerous tissues in the HCCs showing the rim-type fluorescence are negative for NTCP (*left*), whereas increased expression of NTCP is observed in the HCC tissues showing total-type fluorescence (*middle*). Membranous expression of NTCP is observed in the fluorescing part of the HCCs showing partial-type fluorescence (*right*). **c** Immunohistochemical staining of organic anion-transporting polypeptide 8 (OATP8) corresponding to that of NTCP. Membranous expression of OATP8 is also visualized in the fluorescing part of the HCCs showing partial-type fluorescence (*right*), although the expression levels are weak, even in those showing the total-type fluorescence (*middle*). Cancerous tissues in the HCCs showing the rim-type fluorescence are negative for OATP8 (*left*). **d** The degree of OATP8 and NTCP expression levels in the cancerous tissues were higher in the 23 HCCs showing cancerous-type fluorescence of ICG (can) than in the 9 showing rim-type fluorescence (rim)

liver in 6 patients, enabling additional resection of these lesions, all of which were pathologically proven to be HCCs (Fig. 4c). Fluorescence imaging was also useful to confirm the resectability of small HCCs on resected specimens in the operating room (Fig. 4d) (see Supplementary Video 1 and 2).

DISCUSSION

In the present series, fluorescence imaging after preoperative intravenous injection of ICG identified all 276 HCCs on the resected specimens, except three cases of

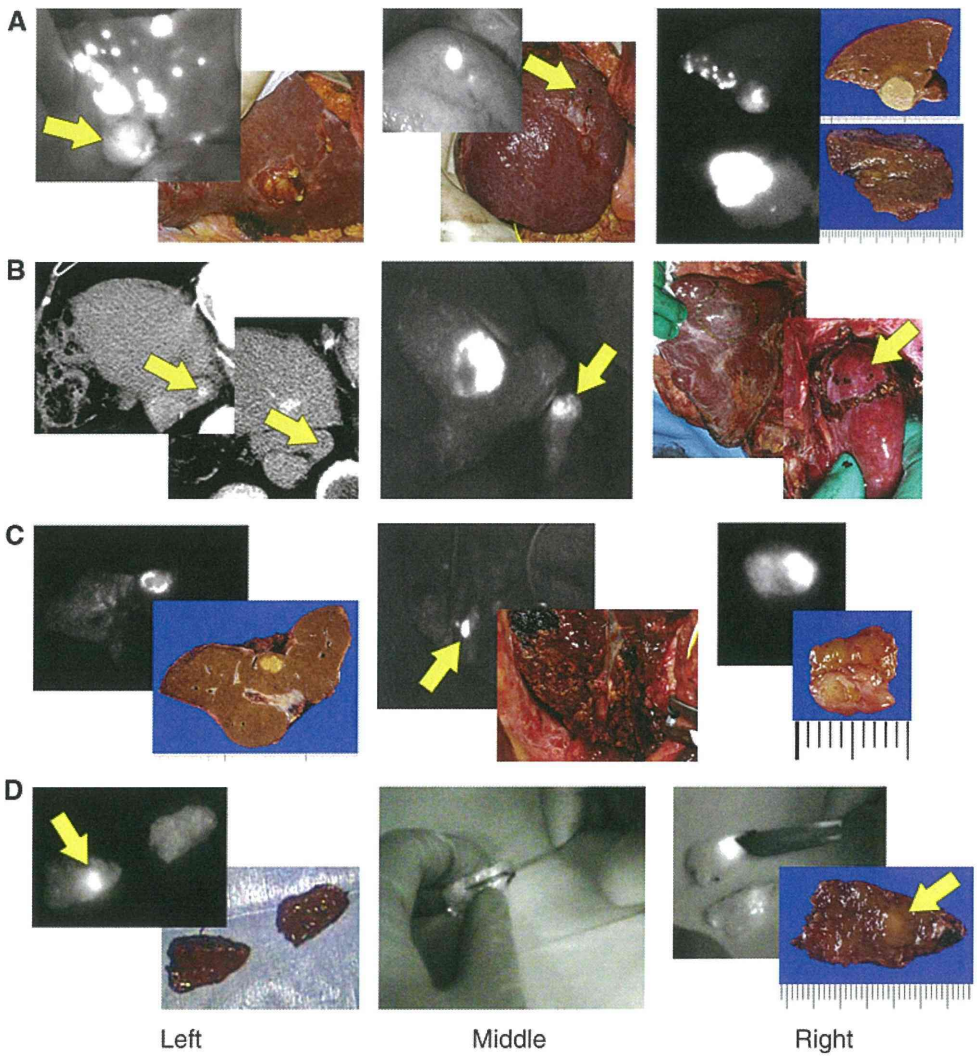

FIG. 4 Clinical applications of indocyanine green (ICG) fluorescence imaging during liver resection. **a** Fluorescence imaging was useful not only for visualization of small intrahepatic metastases scattered around the main tumor (*arrow*, *left*), but also to detect other HCCs developing in a different hepatic segment(s) (*middle*, *arrow*). Fluorescence imaging clearly delineated the intrahepatic metastases and a boundary of secondary tumor with indistinct margin on the resected specimens (*right*). (See Supplementary Video 1a.) **b** Preoperative computed tomography (CT) revealed an HCC in segment I with early enhancement and subsequent washout in portal phase (*arrows*, *left*). Intraoperative fluorescence imaging enabled identification not only of the grossly visible HCC in segment II, but also of the HCC in segment I (*arrow*, *middle*) that could not be identified by visual inspection (*right*), manual palpation, or contrast-enhanced intraoperative ultrasonography (IOUS). (See Supplementary Video 1b.) **c** After right hepatectomy for an HCC showing cancerous fluorescence of ICG on its cut surface (*left*), fluorescence imaging visualized a fluorescing lesion on the wall of the middle hepatic vein where the tumor had been attached (*middle*, *arrow*), enabling additional resection of the remaining HCC tissues (*right*). (See Supplementary Video 2a.) **d** The small hepatic specimen was incised in the operating room to confirm the resectability of the HCC, however, no cancerous tissue was detected (*left*). Because a fluorescing lesion was identified in one of the resected sections (*arrow*, *left*), additional incision was made on the section under the guidance of fluorescence imaging (*middle*), enabling confirmation of resection of the HCC (*arrow*, *right*). (See Supplementary Video 2b.)

HCC in which ICG was administered an exceptionally long time (3 weeks or longer) before surgery. Their fluorescence patterns were associated with the pathological characteristics: the tumors showing fluorescence of ICG in the cancerous tissues (cancerous-type fluorescence, including the total- and partial-type fluorescence) consisted of well- or moderately differentiated HCCs, whereas the majority of tumors showing rim-type fluorescence were poorly differentiated HCCs with microvascular invasion.

Fluorescence microscopy identified the presence of ICG in the canalicular side of the cancer cell cytoplasm and pseudoglands of the HCCs showing a cancerous-type fluorescence pattern and in the non-cancerous liver parenchyma surrounding the HCCs showing the rim-type fluorescence. Gene expression analysis revealed that the expression levels of uptake transporters (*NTCP*, *OATP8*, and *OATP-C*) were well-preserved in HCCs showing a cancerous fluorescence pattern, even in the cancerous

tissues. However, in the HCCs showing rim-type fluorescence, the expression levels of these two genes in the cancerous tissues were considerably lower than those in the corresponding non-cancerous tissues (C/N ratio < 1.0). Immunostaining identified the expression of NTCP and OATP8, the major uptake transporters for ICG,[22] in the cancerous tissues of HCCs showing the cancerous fluorescence pattern, but not in those of HCCs showing the rim-type fluorescence. These results suggest that in differentiated HCC tissues, the portal uptake function is preserved, whereas biliary excretion of ICG is probably impaired because of morphological changes associated with cancer progression rather than functional decrease in biliary transport mainly mediated by MRP2,[2,23] leading to accumulation of ICG in the cancerous tissues after preoperative intravenous administration (Supplementary Fig. 4a–c). Such cancerous-type fluorescence of ICG in differentiated HCC tissues corresponds to the hyper-enhancement of pseudoglandular-type HCC on the hepatobiliary-phase gadoxetic acid-enhanced MRIs, although the mechanism is different, in that gadoxetic acid is taken up by OATP8 and excreted by MRP3.[24] It has also been suggested that most of the poorly differentiated HCCs exhibit rim-type fluorescence on ICG fluorescence images as a result of the impaired portal uptake function in cancerous tissues (Supplementary Fig. 4d). However, further study is needed to confirm whether the ICG accumulation in the non-cancerous liver parenchyma around the tumor is caused only by biliary congestion caused by tumor compression or whether it is also associated with hepatic microenvironmental changes due to cancer progression.

In the clinical setting, the major advantages in ICG fluorescence imaging are its safety and feasibility. ICG use for clinical purposes was approved by the Food and Drug Administration in 1959; [25] thus, the dye has been in clinical use for more than 50 years, with a reported incidence of adverse reactions of less than 0.01 %.[26] Once the ICG retention test is performed within 2–3 weeks prior to surgery for estimation of the acceptable limit of the liver volume to be resected, surgeons can obtain fluorescence images of liver cancers at any time during surgery by simply holding a camera head of the commercially available fluorescence imaging system on the liver surface and resected liver specimens. In contrast, there is a technical limitation in that the tissue penetration depth of the fluorescence emitted by ICG is only 5–10 mm. For more deeply located hepatic lesions, concomitant use of intraoperative IOUS is needed. Another disadvantage is the relatively high incidence of false-positive lesions, especially when ICG is administered only a day before surgery in cirrhotic patients.[4] Our results suggest that newly detected fluorescing lesions with a high FI measuring more than 10 mm are very likely to be HCC, but additional resections for the new lesions should be considered only after they have been adequately confirmed by inspection, palpation, and/or IOUS.

Based on the advantages and disadvantages of ICG fluorescence imaging described above, its major expected role is to delineate: (1) peripherally located HCCs detected by preoperative diagnostic imaging, but unidentifiable by conventional intraoperative diagnostic technique, (2) small HCCs not detected by preoperative diagnostic imaging on the liver surface and resected specimens, (3) cancerous tissues remaining on the raw surface of the liver after resection, and (4) surgical margins for small HCCs with indistinct tumor boundaries (see Supplementary Video 1 and 2). In the present series, ICG fluorescence imaging enabled identification of HCCs that could not be diagnosed preoperatively in 25 of 170 patients (15 %) during liver resection (14 HCCs) and/or macroscopic examination of the resected specimen in the operation room (21 HCCs).

In conclusion, ICG can be taken up by differentiated HCC cells and retained in the cytoplasm and/or pseudoglands for several weeks after intravenous injection, enabling highly sensitive identification of cancerous tissues by intraoperative ICG fluorescence imaging. In other words, the fluorescence imaging technique allows visualization of the pharmacokinetics of organic anions such as ICG in human liver cancer tissues, and could provide valuable information for future development of contrast agents for MRI and photoacoustic tomography,[27] anticancer drugs, and photodynamic treatment using ICG.[28]

ACKNOWLEDGMENT This work was supported by grants from the Takeda Science Foundation, the Kanae Foundation for the Promotion of Medical Science, and the Ministry of Education, Culture, Sports, Science and Technology of Japan (No. 23689060 and No. 23249067). The authors acknowledge the significant contribution made by Drs. N. Harada, S. Tamura, T. Aoki, Y. Sakamoto, and Y. Sugawara, the members of this study group.

DISCLOSURE None.

REFERENCES

1. Stummer W, Stocker S, Wagner S, et al. Intraoperative detection of malignant gliomas by 5-aminolevulinic acid-induced porphyrin fluorescence. *Neurosurgery.* 1998;42:518–5.
2. Kriegmair M, Stepp H, Steinbach P, et al. Fluorescence cystoscopy following intravesical instillation of 5-aminolevulinic acid: a new procedure with high sensitivity for detection of hardly visible urothelial neoplasias. *Urol Int.* 1995;55:190–6.
3. Morton CA, Brown SB, Collins S, et al. Guidelines for topical photodynamic therapy: report of a workshop of the British Photodermatology Group. *Br J Dermatol.* 2002;146:552–7.
4. Ishizawa T, Fukushima N, Shibahara J, et al. Real-time identification of liver cancers by using indocyanine green fluorescent imaging. *Cancer.* 2009;115:2491–504.
5. Gotoh K, Yamada T, Ishikawa O, et al. A novel image-guided surgery of hepatocellular carcinoma by indocyanine green fluorescence imaging navigation. *J Surg Oncol.* 2009;100:75–9.